Seeded growth of highly luminescent CdSe/CdS nano-heterostructures with rod and tetrapod morphologies.

Dmitri V. Talapin,[1,†*] James H. Nelson,[2] Elena V. Shevchenko[1], Shaul Aloni,[1] Bryce Sadtler,[2] and A. Paul Alivisatos[1,2]

[1] *The Molecular Foundry, Lawrence Berkeley National Laboratory, Berkeley, CA 94720*

[2] *Department of Chemistry, University of California, Berkeley, CA 94720*

Corresponding author: D. V. Talapin (dvtalapin@uchicago.edu)

Abstract

We have demonstrated that seeded growth of nanocrystals offers a convenient way to design nano-heterostructures with complex shapes and morphologies by changing the crystalline structure of the seed. By using CdSe nanocrystals with wurtzite and zinc blende structure as seeds for growth of CdS nanorods, we synthesized CdSe/CdS heterostructures nanorods and nano-tetrapods, respectively. Both of these structures showed excellent luminescent properties, combining high photoluminescence efficiency (~80% and ~50% for nanorods and nano-tetrapods, correspondingly), giant extinction coefficients (~$2\cdot10^7$ $M^{-1}cm^{-1}$ and ~$1.5\cdot10^8$ $M^{-1}cm^{-1}$ at 350 nm for nanorods and nano-tetrapods, correspondingly) and efficient energy transfer from the CdS arms into the emitting CdSe core.

† Current address: Department of Chemistry, The University of Chicago, Chicago, IL 60637.

Colloidal synthesis of inorganic nanostructures is developing into a new branch of synthetic chemistry. Starting with preparations of simple objects like spherical nanoparticles [1,2], the field is now moving toward more and more sophisticated structures where size, shape and connectivity of multiple parts of a multicomponent structure can be tailored in an independent and predictable manner [3,4]. Traditional molecular chemistry has proven that synthetic methodology should rely on a toolbox of robust and reproducible techniques. One of the major challenges in the colloidal synthesis of nanomaterials is balancing the two very different processes of nucleation and growth due to their different microscopic mechanisms, reaction orders, etc [5,6]. If the nanoparticle nucleation rate is not properly balanced with the growth rate, i.e., the nucleation rate is either too slow or too fast with respect to the growth rate, the reaction will generate either bulk material or tiny clusters [6,7]. The conditions optimal for nucleating crystalline particles in a homogeneous solution might not be appropriate for tuning nanocrystal size and shape, and vice versa. Moreover, the nucleation stage can yield nuclei with unstable structure inducing phase transitions during nanoparticle growth [8]. For example, the synthesis of nano-tetrapods is based on a delicate balance between stabilities of cubic and hexagonal phases in certain II-VI materials [8,9]. In a narrow window of reaction parameters, CdTe prefers nucleating in a zinc blende structure followed by growth of four "arms" with a wurtzite structure [8]. Balancing all these processes in a one-pot reaction is difficult and leads to strong sensitivity to small variations in reaction conditions. On the other hand, separation of nucleation and growth in colloidal synthesis can be achieved by adding pre-formed nuclei to the reaction mixture. Seeded growth has been successfully implemented in synthesis of core-shell and dumbbell nanocrystals [10-12]. In this letter we demonstrate that both size and structure of the seeds can be used to design multicomponent nanostructures with complex shapes and peculiar optical properties.

Synthesis and properties of CdSe nanocrystals have been extensively investigated over the past two decades. Most classical preparative and spectroscopic studies have been carried out on CdSe nanocrystals with hexagonal (wurtzite) structure, further referred to as "w-CdSe". These can be obtained by reacting cadmium and selenium precursors in the presence of the stabilizing agents trioctylphosphine oxide (TOPO), trioctylphosphine (TOP) and hexadecylamine (HDA) at high temperatures, typically above 300°C [1,13]. Recently CdSe nanocrystals with a cubic (zinc-blende) structure (further referred to as "zb-CdSe") have been synthesized by several groups [14-16]. In this work we compared w-CdSe and zb-CdSe nanocrystals for seeded growth of CdSe/CdS nano-

hererostructures with different morphologies. Combining CdSe and CdS in a single nanostructure creates a material with heterogeneous carrier confinement or "mixed dimentionality" where holes are confined to CdSe while electrons can move freely between CdSe and CdS phases, spreading over the entire nanostructure [11,17]. Previously we synthesized structures consisting of a spherical CdSe nanocrystal connected to a CdS nanorod [17]. In this structures hole is three-dimensionally confined, whereas electron is confined only in two dimensions. Heterostructured CdSe/CdS nanorods exhibited excellent luminescent properties with room temperature photoluminescence quantum efficiencies (PL QE) above 50% and linearly polarized emission. The CdS nanorod can behave as an efficient antenna, absorbing light and funneling the excited carriers into the CdSe core where they radiatively recombine [17]. The very large absorption cross-sections of CdSe/CdS nanorods have been utilized in single-particle luminescence studies [18-21] and LEDs with polarized emission [22]. In addition, CdSe/CdS nanostructures exhibit novel properties originating from the concept of "mixed dimensionality": universal correlation between the spectral linewidth and the position of the excitonic transition in the single particle spectral jitter [18,19], giant Stark effect [20,21], the possibility of manipulating radiative lifetimes by applying an external electric field (exciton storage) [23], etc. Development of CdSe/CdS heterostructures with different morphologies will provide new possibilities for wave function engineering and tailoring optical and optoelectronic properties of semiconductor nanostructures.

We synthesized zb-CdSe nanocrystals via a slightly modified recipe of Cao et al. by reacting cadmium myristate with elemental selenium dissolved in 1-octadecene [15]. zb-CdSe nanocrystals nucleated at 170°C and grew at 240°C in the presence of oleic acid and oleylamine as the capping ligands. The size of zb-CdSe nanocrystal seeds can be tuned by varying the duration of nanocrystal growth at 240°C. w-CdSe nanocrystals capped with HDA, TOPO, TOP and a small amount of n-octyl- or n-tetradecylphosphonic acid have been synthesized as described in Ref. [13]. The detailed synthetic recipes are given in the Experimental Section. Both approaches provide nearly spherical CdSe nanocrystals with size distribution below 10% and sharp excitonic features in the absorption spectra (Figures 1a, b). Both w-CdSe and zb-CdSe nanocrystals form stable colloidal solutions in non-polar solvents like hexane, toluene and TOP, and show narrow PL bands associated with recombination of photoexcited carriers from $1S_h$ and $1S_e$ quantum-confined states. The PL QE of both w-CdSe and zb-CdSe nanocrystals strongly depends on passivation of the nanocrystal surface

with organic ligands, varying between ~3 % and ~30% depending on sample history, e.g., the number of precipitation-redissolution steps applied to purify the nanocrystals from crude solution.

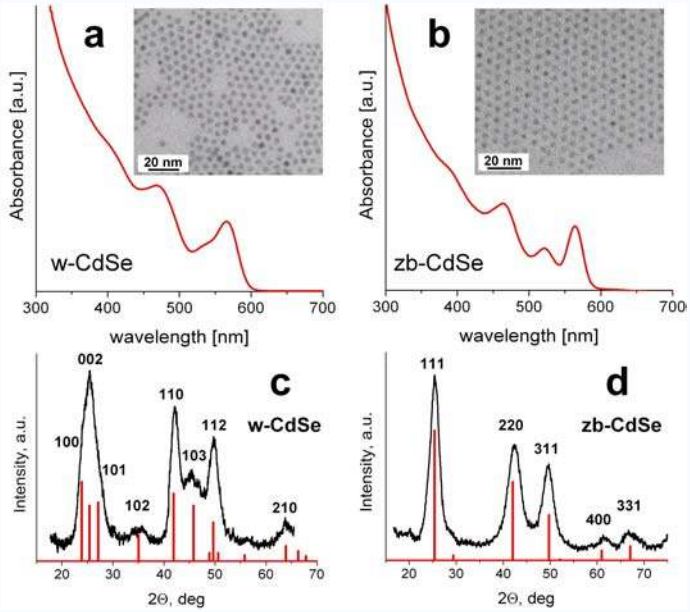

Figure 1. CdSe nanocrystals with wurtzite and zinc blende structures. (a) Absorption spectrum and TEM image of 4.4 nm CdSe nanocrystals with wurtzite lattice. (b) Absorption spectrum and TEM image of 4.0 nm CdSe nanocrystals with zinc blende lattice. (c,d) Powder X-ray (Cu K_α radiation) diffraction patterns of CdSe nanocrystals with wurtzite and zinc blende structures, correspondingly.

Powder X-ray diffraction patterns of w-CdSe and zb-CdSe nanocrystals are shown in Figures 1c,d. The diffraction pattern of w-CdSe nanocrystals shows (102) and (103) reflections at 35.1° and 45.8° 2Θ angles, respectively, characteristic of the wurtzite phase. XRD patterns of zb-CdSe nanocrystals do not show these reflections. Instead, zb-CdSe nanocrystals exhibit a peak at 60.9° which is the (400) reflection of zb-CdSe phase (Figure 1d). The diffraction peak around 25° could be either a convolution of (100), (002) and (101) reflections of w-CdSe phase, or (111) reflection of zb-CdSe phase. In accord with the predictions, this peak in Figure 1c is much broader that (110) and (112) reflections at 42° and 49.7°, whereas in Figure 1d widths of all diffraction peaks are similar. In agreement with previous studies, the (102) and (103) reflections in the XRD patterns of w-CdSe are attenuated because of the presence of stacking faults along the (002) direction - a typical phenomenon in wurtzite II-VI nanocrystals [1]. For additional verification of our structural assignment, we synthesized ~15nm diameter zb-CdSe nanocrystals by additional injections of Cd and Se precursors

at 240°C. The XRD pattern of large CdSe nanocrystals shows narrow diffraction peaks perfectly matching all bulk zb-CdSe reflections. Large CdSe nanocrystals grown at 300°C in the presence of HDA, TOPO and TOP show well-resolved reflections of w-CdSe phase [13].

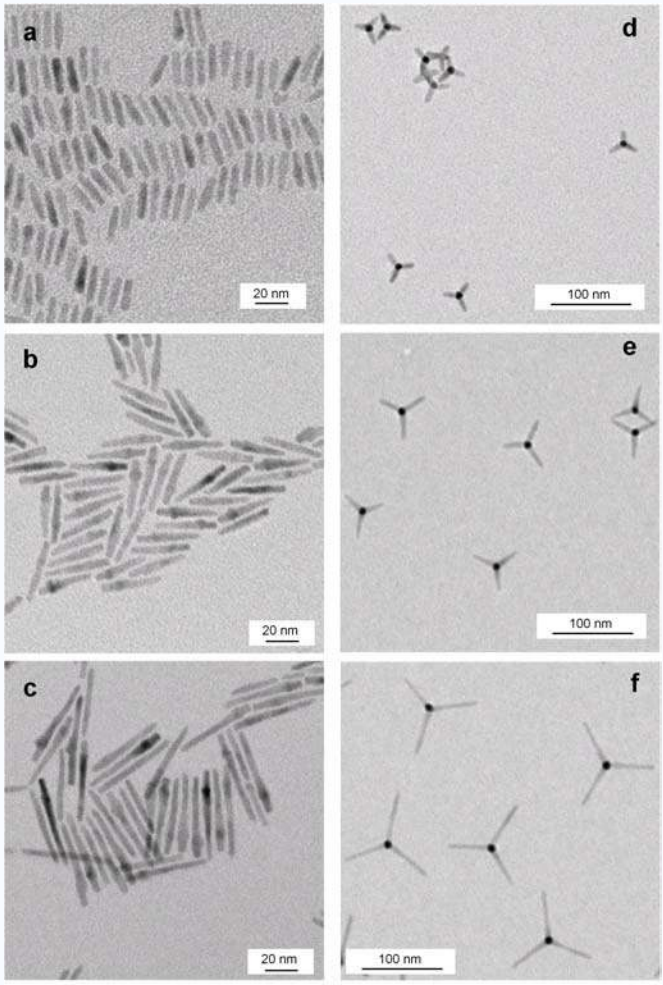

Figure 2. (a-c) TEM images of CdSe/CdS nanorods with different aspect ratios, all grown from 4.4 nm w-CdSe seeds. (d-f) TEM images of CdSe/CdS nano-tetrapods with different lengths of the arms grown from 4.0 nm zb-CdSe seeds.

We injected w-CdSe and zb-CdSe nanocrystals into the reaction mixture containing TOPO, TOP, n-octadecylphosphonic acid (ODPA), n-propylphosphonic acid (PPA), a Cd-ODPA complex and trioctylphosphine sulfide (TOPS) in concentrations optimized for synthesis of high-quality wurtzite-phase CdS (further referred to as "w-CdS") nanorods with long (001) axes (Figure S1) [24]. Low reactivity of the sulfur precursor determines very slow nucleation and growth of the CdS phase

even at high reaction temperatures (320°C). Typically, the nucleation of CdS nanorods starts 2-4 min after the injection of TOPS into the hot reaction mixture due to the high activation barrier for homogeneous nucleation of the CdS phase under these experimental conditions. The solution of CdSe seeds in TOP can be added to the reaction mixture either together with TOPS or 30-60s later, i.e., during the induction period. CdS easily nucleates at the surface of CdSe seeds [11,17]. We found that the structure of the CdSe seeds determined the morphology of CdSe/CdS nano-heterostructures. w-CdSe nanocrystals seeded the formation of CdSe/CdS nanorods (Figure 2a-c) whereas zb-CdSe seeds initiated growth of CdSe/CdS nano-tetrapods (Figure 2d-f). XRD patterns of CdSe/CdS nanorods and nano-tetrapods show that CdS prefer growing in wurtzite phase both from w-CdSe and zb-CdS seeds (Figure S2). The phosphonic acids present in the reaction mixture selectively bind to the {100}-type facets of w-CdS and w-CdSe [25], slowing the nanocrystal growth along these directions and forcing w-CdS to grow along c-axis. The w-CdS phase will primarily nucleate on "polar" {001} and $\{00\bar{1}\}$ facets of w-CdSe seeds, which are structurally identical to fast growing {001} and $\{00\bar{1}\}$ facets of w-CdS [17]. The small mismatch in lattice constants of CdSe and CdS (~3.8% for the {001} planes) is favourable for the epitaxial relation between the CdSe and CdS parts of the nanostructure, observed in HRTEM images (Figure 3a). Analytical scanning electron transmission microscopy (STEM) studies confirmed the presence of CdSe seeds inside CdSe/CdS nanorods. The seed was always shifted toward one end of the nanorod (Figure 3b,c) due to the higher reactivity and faster growth of the $\{00\bar{1}\}$ facet compared to the {001} facet [26]. In long nanorods we often observed an increase in diameter around the CdSe cores (Figure 2b,c) which enables us to compare growth rates for the {001} and $\{00\bar{1}\}$ planes. The distribution of relative facet growth rates within an ensemble of growing nanorods was rather narrow, on the order of 10%. Typically, the $\{00\bar{1}\}$ plane of CdS grew 2-3.5 times faster than the {001} plane. Tailoring the reaction conditions (concentration of w-CdSe seeds, growth time and concentration of sulfur precursor) allowed tuning the length of CdSe/CdS nanorods from 10 nm to ~63 nm, approaching an aspect ratio of ~13. The narrowest length and diameter distributions of the nanorods were observed at injection and growth temperatures of 340°C and 320°C, respectively. The narrow size distribution of the CdSe/CdS nanorods facilitated their self-assembly into superstructures with nematic and smectic ordering (Figures 4a and S3) as well as long-range ordered superlattices (Figure 4b,c). Addition of small amounts of HDA to a solution of CdSe/CdS nanorods in toluene assisted the growth of large superlattice domains with simple-hexagonal packing of nanorods oriented perpendicular to the substrate (Figures 4b,c and S4). Simple

hexagonal packing can be stabilized by dipole-dipole interactions between superlattice building blocks [27].

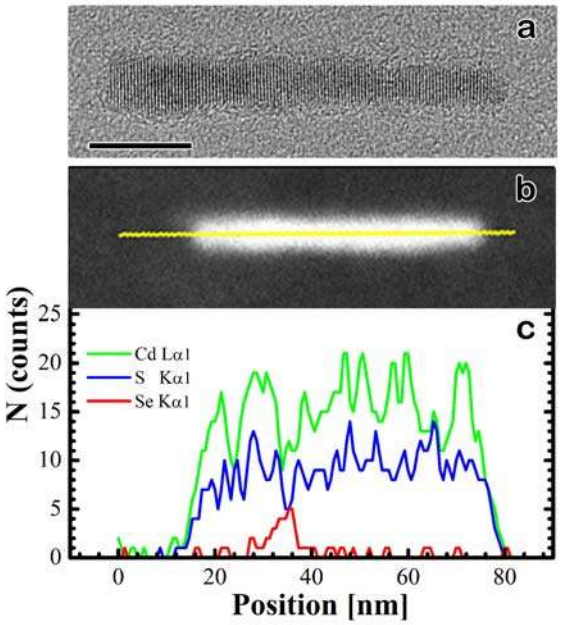

Figure 3. (a) HRTEM image of a CdSe/CdS nanorod grown from a 4.4 nm w-CdSe seed. Scale bar, 5nm. (b) High angle annular dark field (HAADF) image of a CdSe/CdS nanorod and (c) corresponding elemental profiles for Cd, S and Se obtained by recording EDS signal intensities along the line shown in yellow in panel (b).

Analytical STEM studies confirmed the presence of CdSe cores at the branch point of the nano-tetrapods grown from zb-CdSe nanocrystals (Figures 5 and S4). w-CdS nucleated on {111} facets of zb-CdSe nanocrystals which structurally match the fast-growing {001} planes of wurtzite lattice [8,28]. The atomic structure of an interface between the zb-core and the w-arms of CdSe/CdS nano-tetrapod is shown in a HRTEM image of a tetrapod fragment (Figure 5b). HRTEM studies also revealed hexagonal faceting of CdS arms (Figure S5). The length of the tetrapod arms can be tuned from ~5 nm up to ~50 nm by varying the concentration of CdSe seeds while keeping other reaction parameters constant. Lowering the concentration of CdSe seeds results in longer CdS arms. The length and thickness of the arms can be also controlled by adjusting the growth time, typically varied from 10 to 25 min, and the concentration of TOPS in the reaction mixture. Synthesis of CdSe/CdS nano-tetrapods requires precise control of the reaction temperature because zb-CdSe seeds are metastable under the conditions of arm growth. Indeed, the synthesis of CdSe nanocrystals above 300°C in the presence of TOPO, TOP and ODPA yields pure w-CdSe phase. We found that high

injection and growth temperatures (>340°C) results in the formation of significant quantities of arrow shaped nanorods, presumably because of partial transformation of zb-CdSe seeds into w-CdSe. To maximize the yield of nano-tetrapods, we injected TOPS and zb-CdSe seeds at 290-300°C slowly increasing the reaction temperature to 315°C during the arm growth (~1°/min). To reduce the probability of seed phase transformation, we injected zb-CdSe seeds 40-60s after the injection of TOPS, i.e., during the induction period. CdSe/CdS nano-tetrapods can be isolated from the crude solution and reaction byproducts such as CdSe/CdS and CdS nanorods by standard precipitation-dissolution techniques described in the Experimental Section.

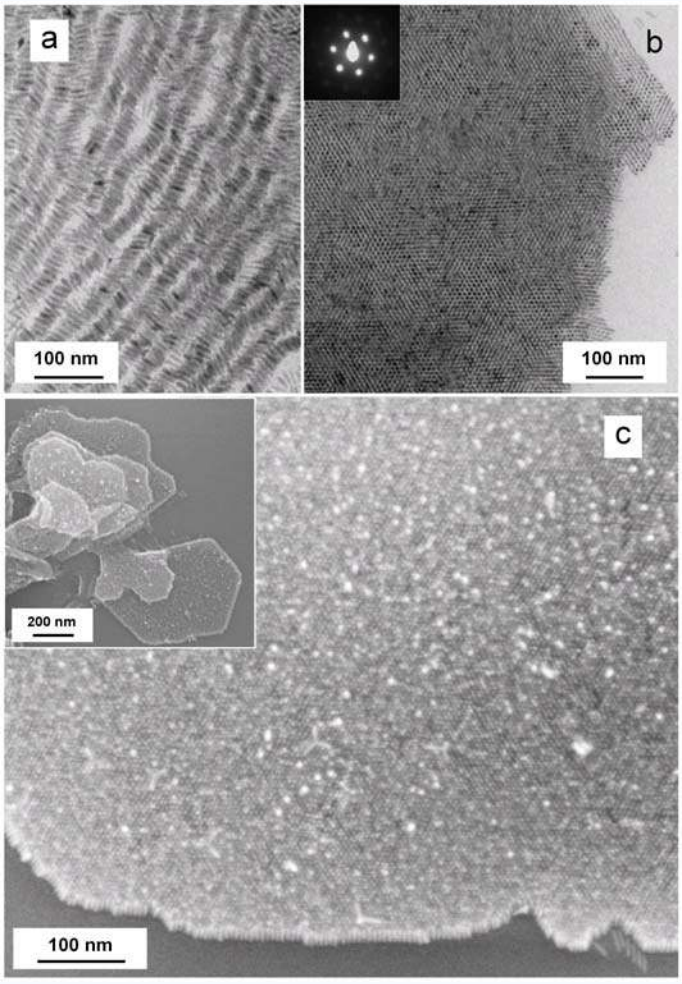

Figure 4. Self-assembly of CdSe/CdS nanorods with length 24 nm and diameter 5.2 nm. (a) TEM image of a superstructure with smectic-A ordering. (b) TEM image of a nanorod superlattice with simple hexagonal packing of nanorods assembled perpendicular to the substrate. Inset shows electron diffraction from a superlattice domain. (c) HRSEM image of CdSe/CdS nanorods assembled perpendicular to the substrate (silicon wafer). Inset shows layer-by-layer growth of a nanorod superlattice.

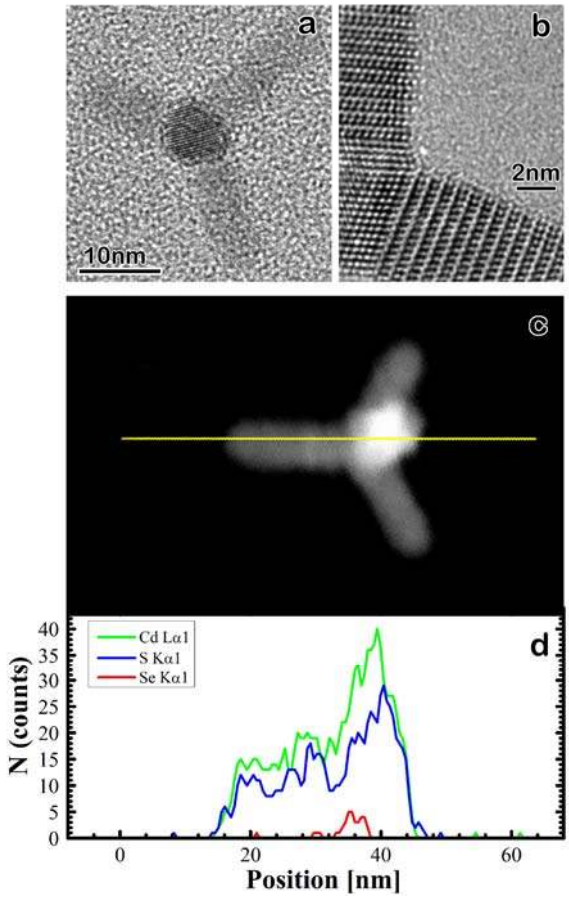

Figure 5. (a) TEM image of a CdSe/CdS nano-tetrapod grown from 4 nm zb-CdSe seed. (b) High-resolution TEM image of a tetrapod fragment showing the interface between {111} planes of zb-CdSe seed and {001} planes of w-CdS arms. (c) High angle annular dark field (HAADF) image of a CdSe/CdS nano-tetrapod and (d) corresponding elemental profiles for Cd, S and Se obtained by recording energy-dispersive X-ray intensities (EDS) along the line shown in yellow in panel (c). Two-dimensional elemental map of a CdSe/CdS nano-tetrapod is shown in Figure S4 from Supporting Information.

Both CdSe/CdS nanorods and nano-tetrapods form stable and optically clear colloidal solutions in toluene, hexane and other non-polar organic solvents. The optical absorption spectra of CdSe/CdS nanorods and nano-tetrapods, both grown from the CdSe seeds having the first excitonic transition at 563-565 nm show two characteristic features: the peaks in the red part of the spectrum associated with the CdSe core and very steep absorption onset below 500 nm, characteristic to the absorption by the CdS parts of the nanostructure (Figure 6a,b). Delocalization of the electron and hole wave functions into CdS results in a red shift of excitonic peaks in the CdSe/CdS heterostructures, thereby

shifting the first excitonic maximum in absorption spectrum of 46 nm long, 4.4 nm diameter CdSe/CdS nanorods from 565 nm to 609 nm. In nano-tetrapods with similar arm diameter the red shift is significantly larger, the first excitonic peak shifts from 563 nm to 623 nm upon growth of 25 nm long CdS arms. Larger red shift in heterostructures with tetrapod morphology compared to nanorods can originate both from the intrinsic difference in energy levels of w-CdSe and zb-CdSe seeds and shape effects on electronic states in these nanostructures [31].

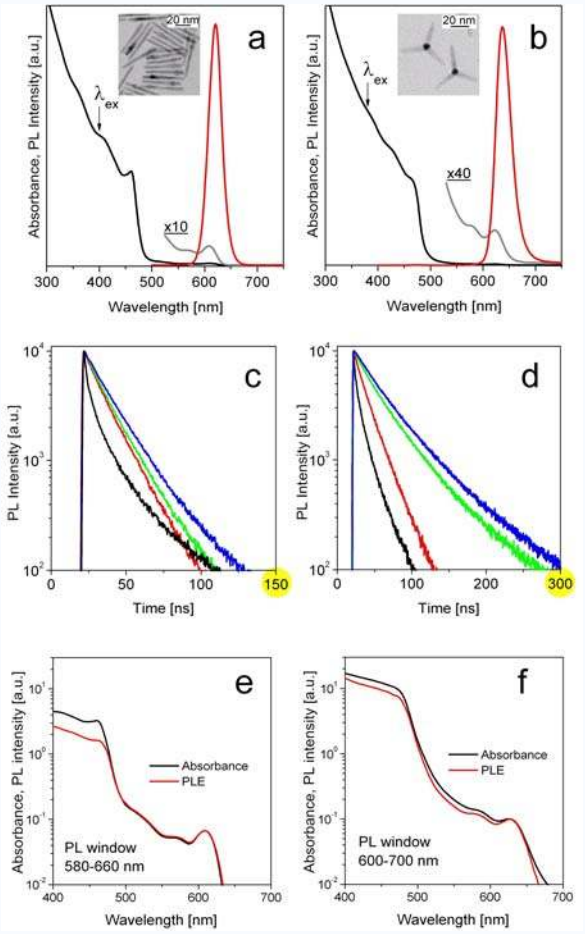

Figure 6. (a) Absorption (black) and PL (red) spectra of toluene solutions of 46 nm long CdSe/CdS nanorods grown from 4.4 nm w-CdSe seeds. Gray line shows magnified absorption spectrum to emphasize structure of the absorption onset. Absolute PL quantum efficiency of this sample was 80%, measured at the excitation wavelength 514 nm. **(b)** Absorption (black) and PL (red) spectra of toluene solutions of CdSe/CdS nano-tetrapods with 24 nm CdS legs grown from 4 nm zb-CdSe seeds. Gray line shows magnified absorption spectrum to emphasize structure of the absorption onset. Absolute PL quantum efficiency of this sample was 39%, measured at at the excitation wavelength 512 nm. **(c)** Fluorescence decay of 4.4 nm w-CdSe nanocrystals (black) and CdSe/CdS nanorods with different lengths: 12.2 nm (red), 24 nm (green), 36 nm (blue). All samples were excited at 440 nm; emission was detected at the maxima of the PL spectra. **(d)** Fluorescence decay of 4.0 nm zb-CdSe

nanocrystals (black) and CdSe/CdS nano-tetrapods with arm length of 9.2 nm (red), 24 nm (green), 38 nm (blue). All samples were excited at 440 nm; emission was detected at the maxima of the PL spectra. **(e)** Comparison of Absorption and PL excitation spectra for 46 nm CdSe/CdS nanorods shown in panel (a). PL intensity was integrated throughout the entire emission band. Absorbance in the first excitonic maximum was normalized to 0.1. **(f)** Comparison of Absorption and PL excitation spectra for CdSe/CdS nano-tetrapods with 24 nm long CdS arms shown in panel (b). PL intensity was integrated throughout the entire emission band. Absorbance in the first excitonic maximum was normalized to 0.1.

Below 500 nm CdS provide the major contribution to the absorption of our CdSe/CdS nanostructures. The dominance of the arm absorption is most pronounced in the case of nano-tetrapods where the absorption of the CdSe cores can barely be seen without zooming in to the red part of the absorption spectrum (Figure 6b). In nano-tetrapods with 50 nm long arms the absorption cross-section of the CdS arms is ~300 times larger than the absorption cross-section of the CdSe core (Figure S6), implying that more than 99% of the incident light is absorbed by the arms of the tetrapod. The CdSe-related absorption peaks can be used as an internal standard to calculate the molar extinction coefficient (ε) of CdSe/CdS nanorods and nano-tetrapods. Our earlier studies revealed that the oscillator strength of the first excitonic transition in CdSe/CdS nanorods is comparable to that of bare CdSe cores [17,30]. 4.4 nm w-CdSe nanocrystals have $\varepsilon \sim 2.5 \cdot 10^5$ $M^{-1}cm^{-1}$ at the first absorption maximum [31]. We obtained similar values (±30%) for ε of bare zb-CdSe nanocrystals. Thus, 46 nm long CdSe/CdS rods have $\varepsilon \sim 2 \cdot 10^7$ $M^{-1}cm^{-1}$ at 350 nm and $\varepsilon \sim 4 \cdot 10^7$ $M^{-1}cm^{-1}$ at 300 nm. These impressive values look small when compared to extinction coefficients of the nano-tetrapods which have ε above 10^8 $M^{-1}cm^{-1}$! Our estimates for a solution of tetrapods with ~50 nm long CdS arms give $\varepsilon \sim 1.5 \cdot 10^8$ $M^{-1}cm^{-1}$ at 350 nm and $\varepsilon \sim 3 \cdot 10^8$ $M^{-1}cm^{-1}$ at 300 nm. The absorption cross-section of individual arms of a tetrapod (e.g., CdS nanorods) should be strongly dependent on their orientations with respect to polarization of incoming photons. However, four CdS nanorods arranged around a CdSe core in form of tetrapod arms form a perfect antenna which effectively captures photons coming from *any* direction and with *any* polarization, leading to giant absorption cross-section of the entire construction.

CdSe/CdS nanorods and nano-tetrapods exhibit luminescence with high quantum yield. They can emit in the yellow, orange or red part of the spectrum, depending on the size of CdSe seed and diameter of CdS rods, whereas the length of the nanorod or tetrapod arms has a minor effect on the emission wavelength. Spectral position of the emission band shows that the radiative recombination

of photoexcited carriers occurs in the CdSe core, whereas the emission of CdS arms is strongly suppressed (Figure 6a,b). The global Stokes shift observed for our CdSe/CdS nanorods is ~41-46 meV, nearly independent of the nanorod length [32], whereas the Stokes shift in nano-tetrapods is larger, approaching ~78 meV, and rises with increasing length of the CdS arms. The room temperature PL quantum efficiencies of the CdSe/CdS nanorods were typically 75-80%. The error of our PL QE measurements was found to be ≤10% and has been verified by using a series of laser dyes emitting in different parts of the spectrum (Rhodamine 6G, Rhodamine 640, LD 690) and measuring their PL efficiencies with respect to each other. In contrast to bare CdSe nanocrystals whose PL QE is strongly dependent on sample history, washing the nanorods from the crude solution by several precipitation/redissolution steps did not result in significant drops in the PL efficiency. We routinely observed PL QEs above 75% after two purification stages. Time-resolved PL measurements show nearly linear fluorescence decays (Figure 6c), characteristic of a single dominant recombination channel and a reduced role of trapping-detrapping processes at the nanorod surface. The radiative decay rate gradually decreased with increasing nanorod length (Figure 6c), as expected because of the reduced oscillator strength due to the decreased electron – hole wave function overlap [20]. Bare w-CdSe seeds show fast non-linear decay because of presence of non-radiative recombination channels.

The PL QEs of the CdSe/CdS nano-tetrapods were typically between 35% and 60%. Generally, the samples with skinnier arms exhibited higher PL efficiencies compared to the tetrapods with "fat" arms while the length of the arms had a minor effect on the PL QE. CdSe/CdS nano-tetrapods showed significantly larger PL lifetimes compared to CdSe/CdS nanorods with similar arm diameter (Figure 6d). To understand this result, the photophysics of zb-CdSe nanocrystals has to be studied. To the best of our knowledge, there were no experimental studies of the electronic structure and the emitting state in the zb-CdSe nanocrystals. Our preliminary results show lower radiative rates for zb-CdSe nanocrystals compared to w-CdSe ones, estimated as $\tau_{rad}^{-1} = (PL\ QE)/\tau_{PL}$ where τ_{PL} is approximated as 1/e PL decay time: 6.7ns and 9.3ns for w-CdSe and zb-CdSe nanocrystals, correspondingly. The crystal field can induce large perturbations to the electronic structure in nanocrystals with significant shape anisotropy. Semiempirical pseudopotential calculations by Li and Wang showed that the lowest electronic state in a nanocrystal with tetrapod morphology is completely localized in the central tetrahedron while the first hole state is more delocalized and is present in the arms of the tetrapod [29]. In CdSe/CdS tetrapod-heterostructures where the hole is localized in CdSe by the valence band offset, we should expect localization of both electron and hole

states in the center of the tetrapod, maximizing the wave function overlap and leading to high luminescence efficiency. Quantum confinement in narrow-arm tetrapods should result in a higher degree of localization of the electron wave function at the branch point. In accord with this prediction, we observed an increase of the radiative rate in tetrapods with decreasing arm diameter.

CdSe/CdS nanorods and tetrapods have giant absorption cross-sections below 500 nm due to the efficient light absorption by the CdS arms. Our earlier studies demonstrated very efficient charge transfer from the CdS rod to the emitting CdSe core [17]. To quantify the efficiency of transfer from CdS to CdSe in heterostructures with different morphologies, we measured PL excitation (PLE) spectra. We observed quantitative agreement between absorption and PLE spectra for short (<20nm) CdSe/CdS nanorods demonstrating that eventually all electron-hole pairs generated in CdS are captured by the w-CdSe core. In the case of long (46 nm) rods some portion of the photoexcited carriers recombine in the CdS arms, as evidenced from the difference between absorption and PLE spectra below 465 nm (Figure 6e) and the appearance of a very weak emission band around 470 nm. In case of nano-tetrapods with similar absorption cross-section, the travel path from the CdS arms into the emitting zb-CdSe core is about four times shorter, resulting in more efficient carrier collection. Indeed, we observed nearly quantitative agreement between absorption and PLE spectra of the nano-tetrapods with 24 nm long arms (Figure 6f). The combination of a giant absorption cross-section and efficient energy transfer from CdS arms into highly emitting CdSe core places CdSe/CdS nano-tetrapods among the best light harvesting systems and makes is particularly useful for various applications such as light concentrators, solar cells, LEDs. Four CdS arms of a tetrapod can be used for pumping carriers into the CdSe core, leading to lower lasing thresholds. Further interesting results are likely to come from spectroscopic studies of single CdSe/CdS nano-tetrapods that are currently underway.

In summary, we have demonstrated an efficient way of engineering the shape of nanocrystal heterostructures by tailoring the phase of the nanocrystal seeds. These results should be considered as a significant step on the way toward controllable synthesis of complex multicomponent nanostructures with precisely designed physical and chemical properties.

Supporting Information Available. TEM images of CdS nanorods grown in the absence of CdSe seeds (Figure S1); X-ray diffraction patterns of CdSe/CdS nanorods and nano-tetrapods (Figure S2); TEM images of CdSe/CdS nanorods self-assembled into a superstructure with nematic and

simple-hexagonal ordering (Figure S3); Two-dimensional elemental map for a nano-tetrapod obtained from analytical TEM (Figure S4); HRTEM of a CdSe/CdS nano-tetrapod (Figure S5); Absorption and PL spectra of CdSe/CdS nano-tetrapods with 50 nm long arms (Figure S6).

Acknowledgements. We thank S. Claridge and P. Guyot-Sionnest for stimulating discussions and T. Mattox for technical support. Work at the Molecular Foundry was supported by the Director, Office of Science, Office of Basic Energy Sciences, Division of Materials Sciences and Engineering, of the U.S. Department of Energy under Contract No. DE-AC02-05CH11231.

Experimental details

Wurtzite CdSe nanocrystals:
10.0 g (25.9 mmol) TOPO and 5.00 g (20.7 mmol) HDA were loaded into a 50 mL three-neck flask and heated to 110 °C for 50 min under vacuum. Under flow of N_2, either 0.400 g (1.52 mmol) TDPA or 0.300 g (1.68 mmol) OPA were quickly added and the reaction was degassed under vacuum for another 5 min. Reaction mixtures with TDPA produced smaller nanoparticles, whereas mixtures with OPA allowed for growth of particles with diameters above 4.5 nm. The reaction mixture was heated to 300 °C under flowing N_2 and an injection solution of 1 mmol TOPSe and 1.64 mmol dimethylcadmium dissolved in 5 mL TOP was rapidly injected into the stirring mixture. Additional injections of stock solution to reactions containing OPA were necessary to grow particles larger than 5 nm. Reactions were kept at 300 °C under flowing N_2 overnight, at which time they were cooled to room temperature and opened to air. The resulting solid was transferred into the glovebox and dissolved in anhydrous toluene. The vial was centerfuged to remove any solids and the subsequent mixture was precipitated with anhydrous ethanol and resuspended in anhydrous toluene.

Zinc blende CdSe nanocrystals:
In a 100 mL three-neck flask, 0.34 g (0.6 mmol) cadmium myristate were dissolved in 37 mL 1-octadecene and degassed upon heating at 90 °C under vacuum for 40 min. The solution was cooled to room temperature and 0.024 g (0.3 mmol) 100 mesh Se powder (99.999%) were added to the reaction mixture, followed by degassing at 50 °C under vacuum for 10 min. The reaction mixture was heated to 240°C (~24 deg/min) under N_2 atmosphere. zb-CdSe nanocrystals nucleated at ~170°C, observed through the change of the solution color from colorless to yellow. The reaction temperature was allowed to rise up to 240°C. A degassed solution of 0.1 mL oleic acid and 1 mL oleylamine in 4 mL 1-octadecene was added dropwise to the reaction mixture ~3 min after approaching 240°C to stabilize the nanoparticle growth. The growth of nanocrystals can be visually monitored by change of solution color from yellow to deep red and taking aliquots for UV-Vis and PL measurements. Typically, it took zb-CdSe nanocrystals ~2 hrs to grow from initial nuclei to 5 nm diameter nanocrystals. Larger nanocrystals can be synthesized by additional injections of Cd and Se precursors to the reaction mixture at 240°C. After cooling the reaction mixture to room temperature, zb-CdSe nanocrystals were precipitated by adding ethanol or acetone to the crude solution, transferred to a glovebox and re-dispersed in unhydrous hexane. The purification step can be repeated several times by using different solvent/nonsolvent combinations.
Cadmium myristate can be synthesized as described in ref. [15] or prepared *in situ* by reacting 0.077 mg CdO with 0.29 g myristic acid in 5 mL 1-octadecene at 250 °C followed by the addition of 32 mL 1-octadecene and degassing the solution at 80°C under vacuum for 1 hr

Preparation of stock solutions of w-CdSe and zb-CdSe seeds:
The concentration of w-CdSe nanocrystals was calculated using the size dependent molar extinction coefficient given in refs. [31,33]. Particle size was determined by the position of the first exciton peak maximum as given in the supporting information to ref. [34].
We could not find information about the size dependent molar extinction coefficients for zb-CdSe nanocrystals. To calculate the concentration of our zb-CdSe seed solutions, we thoroughly purified colloidal solutions of zb-CdSe nanocrystals by 5-6 precipitation/re-dissolution steps under inert atmosphere using different combinations of anhydrous solvents and non-solvents (hexane/acetone, hexane/ethanol, toluene/methanol, toluene/acetonitrile, chloroform/methanol,

chloroform/acetone, etc) to purify the nanocrystals from any residual precursors and high boiling solvents. Then, zb-CdSe nanocrystals were dissolved in anhydrous hexane, filtered through a 0.2 μm PTFE filter. We measured weight of the nanocrystals after evaporating hexane and correlated it with absorbance of nanocrystals. This procedure allowed us to estimate the molar extinction coefficient of zb-CdSe nanocrystals which was found similar to that of w-CdSe nanocrystals within ~30% error bar introduced by the surface ligands.

Solutions for synthesis of CdSe/CdS nanorods and nano-tetrapods:
0.207 g (1.61 mmol) CdO, 1.08 g (3.23 mmol) n-octadecylphosphonic acid (Polycarbon, 99%), 0.015 g (0.12 mmol) n-propylphosphonic acid, and 3.35 g (9.18 mmol) TOPO (Aldrich Reagent Plus, 99%) were loaded into a 25 mL three-neck flask and heated to 120 °C for 30 min under vacuum. The mixture was heated to 320 °C under flowing N_2 to produce an optically clear solution. After the CdO completely dissolved, the solution was cooled to 120 °C and put under vacuum for 2 h, after which it was heated to 340°C (for nanorod synthesis) or 300°C (for nano-tetrapod synthesis) under flowing N_2. At this time 1.5 g (4.05 mmol) TOP (Strem, 97%) was injected and the flask was allowed to return to 340°C (for nanorod synthesis) or 300°C (for nano-tetrapod synthesis).

TOPS was prepared by reacting equimolar amounts of TOP and elemental sulfur at 50 °C under inert atmosphere.

Synthesis of CdS/CdSe rods:
0.65 g TOPS (1.61 mmol) was injected into the Cd/ODPA/PPA/TOPO/TOP solution at 340°C, followed after 20 s by the injection of ~10^{-8} mol w-CdSe seeds (~2mg CdSe in case of 4.4 nm nanocrystals) dissolved in 0.50 g (1.35 mmol) TOP. The w-CdSe solution was prepared by concentrating 1 mL of 10^{-5} M solution of w-CdSe nanocrystals in toluene under vacuum to ~0.05 mL and adding 0.5 g TOP (gentle sonication might be necessary to disperse the CdSe nanocrystals in TOP). The reaction temperature was adjusted to 320 °C and after 10 min the reaction was stopped by injection of 10 mL anhydrous toluene and removal of the heating mantle. Once the flask reached room temperature it was opened to air. CdSe/CdS nanorods can be isolated by mixing crude solution with toluene (~1:1 by volume) and adding ethanol - to induce flocculation – followed by centrifugation to precipitate the nanorods. Precipitated nanorods were redispersed in hexane:octylamine (8:1 by volume) mixture and precipitated again with ethanol. The resulting CdS/CdSe nanorods formed stable colloidal solutions in toluene and exhibited bright and stable luminescence in air for months.

The above recipe produced 46 ± 9 nm rods with a small bump on one side indicating the position of the CdSe dot inside the rod. The diameter of these rods as measured at the center of the rod's length was 4.2 ± 0.5 nm. Modifications to this synthetic procedure allow for control of nanorod length and diameter. The diameter and length of the rods could be controlled by the amount of TOPS injected into the reaction – more TOPS producing longer and skinnier rods, with 0.330g TOPS giving rods of length 24 ± 2 nm of diameter 5.2 ± 0.5 nm, or with 1.30g TOPS giving rods with length 55 ± 12 nm and of diameter 4.2 ±0.5 nm. Also, the length of the rods could be controlled by injection of different amounts of CdSe dots – more dots producing shorter rods, with $3.0 \cdot 10^{-8}$ mol of dots giving rods of length 22 ± 4 nm and of diameter 5.2 ± 0.7 nm. Finally, the reaction growth time could be changed to control rod length – longer times producing longer rods, with 3 min growth giving rods of length 12 ± 1 nm and diameter 4.7 ± 0.5 nm.

CdS/CdSe tetrapods:
0.65 g TOPS was injected into the Cd/ODPA/PPA/TOPO/TOP solution at 300°C, followed after 40 s by the injection of zb-CdSe seeds (2mg zb-CdSe nanocrystals, ~10^{-8} mol of 4.0 nm nanocrystals) dissolved in 0.50 g TOP. The zb-CdSe solution was prepared by mixing 0.5 mL of 4 mg/mL solution of 4.0 nm zb-CdSe nanocrystals in hexane with 0.5 g TOP followed by evaporating hexane under vacuum. The reaction temperature was increased to 315 °C (~1 deg/min). The growth of CdS arm continued for 15 to 25 min and was stopped by cooling the reaction mixture to room temperature. The length of tetrapod arms was varied by adjusting the concentration of zb-CdSe seeds. Thus, 6 mg, 4 mg, 2 mg, 1 mg of 4.0 nm zb-CdSe seeds yielded CdSe/CdS nano-tetrapods with arm lengths of 15 nm, 19 nm, 24 nm and 46 nm, correspondingly. Longer growth time typically resulted in increasing the diameter of CdS arms. As-synthesized CdSe/CdS nano-tetrapods can be isolated by adding toluene to the crude solution and flocculating the tetrapods with acetone. The precipitate was re-dispersed in hexane:octylamine (8:1 by volume) mixture and precipitated with acetone (~8:6 hexane-to-acetone ratio). Collected precipitate can be redispersed in toluene or hexane. Often the as-synthesized nano-tetrapods contain some impurities such as CdSe/CdS and CdS nanorods. These can be separated from nano-tetrapods by size- and shape-selective precipitation. We centrifuged solutions of tetrapods in toluene at 12000g for 15 min. Since the tetrapods are significantly heavier than nanorods, they concentrated at the bottom of centrifugation tube. The supernatant was carefully removed and the concentrated tetrapod solution was diluted with toluene. Repeating this procedure two times allowed us to remove nanorods and other reaction by-products

References

1. Murray, C. B.; Norris, D. J.; Bawendi, M. G. *J. Am. Chem. Soc.* **1993**, *115*, 8706.
2. Brust, M.; Walker, M.; Bethell, D.; Schiffrin, D. J.; Whyman, R.J. *Chem.Commun.* **1994**, 801.
3. Milliron, D. J.; Hughes, S. M.; Cui, Y.; Manna, L.; Li, J.; Wang, L.-W.; A. P. Alivisatos. *Nature* **2004**, *430*, 190.
4. Yin, Y.; Alivisatos, A. P. *Nature* **2005**, *437*, 664.
5. Sugimoto, T. *Adv. Colloid Interfac. Sci.* **1987**, *28*, 65.
6. Shevchenko, E. V.; Talapin, D. V.; Schnablegger, H.; Kornowski, A.; Festin, O.; Svedlindh, P.; Haase, M.; Weller, H. *J. Am. Chem. Soc.* **2003**; *125*; 9090.
7. Yu, W. W.; Peng, X. *Angew. Chem. Int. Ed.* **2002**, *41*, 2368.
8. Manna, L.; Milliron, D.; Meisel, A.; Scher, E. C.; A. P. Alivisatos. *Nat Mater.* **2003**, *2*, 382.
9. Carbone, L.; Kudera, S.; Carlino, E.; Parak, W. J.; Giannini, C.; Cingolani, R.; Manna, L. *J. Am. Chem. Soc.* **2006**; *128*; 748.
10. Hines, M. A.; Guyot-Sionnest, P. *J. Phys. Chem.* **1996**, *100*, 468.
11. Peng, X.; Schlamp, M. C.; Kadavanich, A.; Alivisatos, A. P. *J. Am. Chem. Soc.* **1997**, *119*, 7019.
12. Yu, H.; Chen, M.; Rice, P. M.; Wang, S. X.; White, R. L.; Sun, S. *Nano Lett.* **2005**; *5*; 379.
13. Talapin, D. V.; Rogach, A. L.; Kornowski, A.; Haase, M.; Weller, H. *Nano Letters* **2001**, *1*, 207.
14. Rogach, A. L.; Kornowski, A.; Gao, M.; Eychmuller, A.; Weller, H. *J. Phys. Chem. B.* **1999**; *103*; 3065.
15. Yang, Y. A.; Wu, H.; Williams, K. R.; Cao, Y. C. *Angew. Chem. Int. Ed.* **2005**, *44*, 6712.
16. Han, L.; Qin, D.; Jiang, X.; Liu, Y.; Wang, L.; Chen, J.; Cao, Y. *Nanotechnology* **2006**, *17*, 4736.
17. Talapin, D. V.; Koeppe, R.; Götzinger, S.; Kornowski, A.; Lupton, J. M.; Rogach, A. L.; Benson, O.; Feldmann, J.; Weller H. *Nano Letters* **2003**, *3*, 1677.
18. Müller, J.; Lupton, J. M.; Rogach, A. L.; Feldmann, J.; Talapin, D. V.; Weller, H. *Phys. Rev. Lett.* **2004**, *93*, 167402
19. Müller, J.; Lupton, J. M.; Rogach, A. L.; Feldmann, J.; Talapin, D. V.; Weller, H. *Phys. Rev. B* **2005,** *72*, 205339.

20. Muller, J.; Lupton, J. M.; Lagoudakis, P. G.; Schindler, F.; Koeppe, R.; Rogach, A. L.; Feldmann, J.; Talapin, D. V.; Weller, H. *Nano Lett.* **2005**; 5; 2044.
21. Becker, K.;Lupton, J. M.; Müller, J.; Rogach, A. L.; Talapin, D. V.; Weller, H.; Feldmann, J. *Nat. Mater.* **2006**, *5*, 777.
22. Hikmet, R. A. M.; Chin, P. T. K.; Talapin, D. V.; Weller, H. *Adv. Mater.* **2005**, *17*, 1436.
23. Kraus, R. M.; Lagoudakis, P. G.; Rogach, A. L.; Talapin, D. V.; Weller, H.; Lupton, J. M.; Feldmann, J. *Phys Rev. Lett.* **2007**, *98*. 017401.
24. Robinson, R. D.; Sadtler, B.; Demchenko, D. O.; Erdonmez, C. K.; L.-W. Wang, A. P. Alivisatos. *Science*, **2007**, *317*, 355.
25. Li, J.; Wang, L.-W. *Nano Lett.* **2003**, *3*; 1357.
26. Manna, L.; Scher, E. C.; Alivisatos, A. P. *J. Am. Chem. Soc.* **2000**; *122*; 12700.
27. Talapin, D. V.; Shevchenko, E. V.; Murray, C. B.; Titov, A. V.; Kral, P. *Nano Lett.* **2007**; *7*; 1213.
28. Xie, R.; Kolb. U.; Basche, T. *Small* **2006**, *2*, 1454.
29. Manna, L.; Wang, L. W.; Cingolani, R.; Alivisatos, A. P. *J. Phys. Chem. B.* **2005**; *109*; 6183.
30. Talapin, D. V.; Shevchenko, E. V.; Murray, C. B.; Kornowski, A.; Forster, S.; Weller, H. *J. Am. Chem. Soc.* **2004**; *126*; 12984.
31. Yu, W. W.; Qu, L.; Guo, W.; Peng, X. *Chem. Mater.* **2003**; *15*; 2854.
32. This observation appears to contradict our data obtained on shorter CdSe/CdS nanorods synthesized at 120°C using HDA and TOPO as the capping ligands [17]. The inconsistency could originate from a structural difference between CdSe/CdS nanorods synthesized at 320°C and capped with ODPA and those grown at 120°C in the presence of HDA: at 320°C CdS nucleates and grows both on {001} and $\{00\bar{1}\}$ facets of the w-CdS seed whereas at 120°C we observed the growth of CdS rod solely from the $\{00\bar{1}\}$ facet. Moreover, at 320°C partial alloying of CdSe and CdS phases can take place.
33. Leatherdale, C. A.; Woo, W.-K.; Mikulec, F. V.; Bawendi, M. G., *J. Phys. Chem. B*, **2002**, *106*, 7619.
34. Mikulec, F. V.; Kuno, M.; Bennati, M.; Hall, D. A.; Griffin, R. G.; Bawendi, M. G. *J. Am. Chem. Soc.* **2000**, *122*, 2532.

TOC Graphic

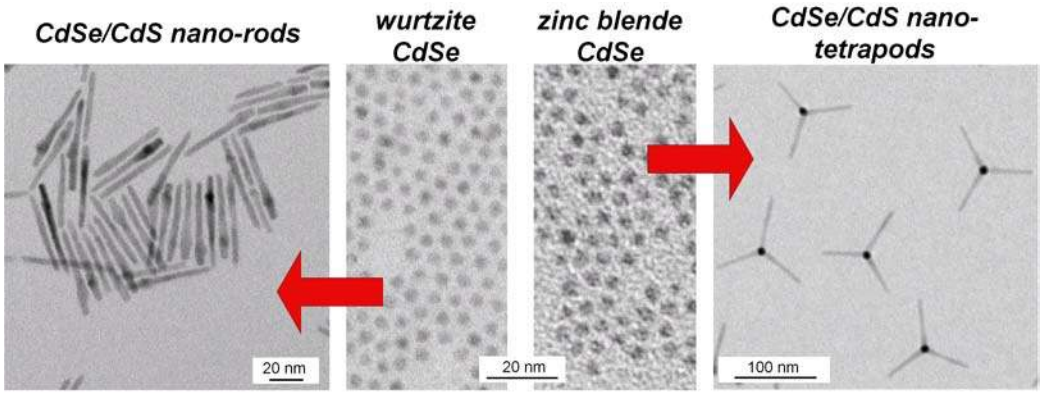
CdSe/CdS nano-rods
wurtzite CdSe
zinc blende CdSe
CdSe/CdS nano-tetrapods
20 nm
20 nm
100 nm

Supporting Information

Seeded growth of highly luminescent CdSe/CdS nano-heterostructures with rod and tetrapod morphologies.

Dmitri V. Talapin,[1,‡*] James H. Nelson,[2] Elena V. Shevchenko[1], Shaul Aloni,[1] Bryce Sadtler,[2] and A. Paul Alivisatos[1,2]

[1] *The Molecular Foundry, Lawrence Berkeley National Laboratory, Berkeley, CA 94720*

[2] *Department of Chemistry, University of California, Berkeley, CA 94720*

Corresponding author: D. V. Talapin (dvtalapin@uchicago.edu)

[‡] Current address: Department of Chemistry, The University of Chicago, Chicago, IL 60637.

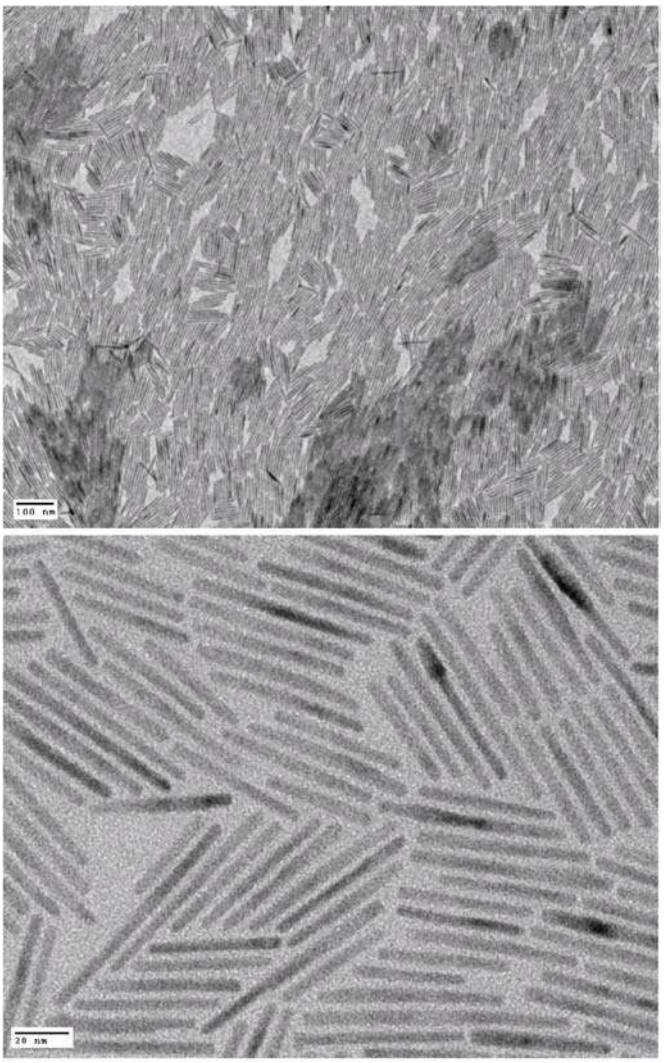

Figure S1. TEM images of CdS nanorods formed in the absence of CdSe seeds.

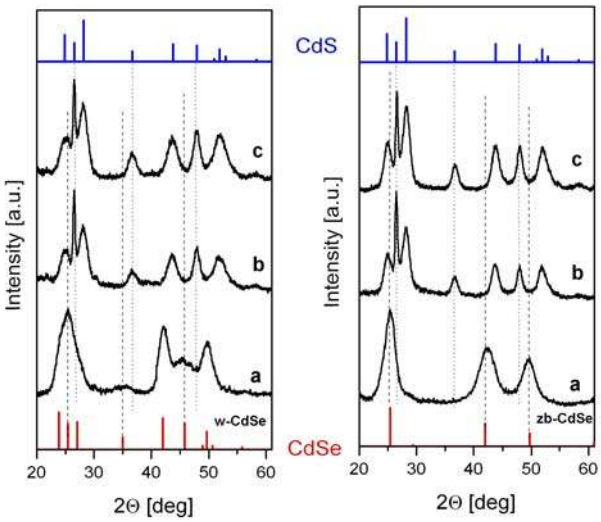

Figure S2. (left) Powder X-ray diffraction spectra of w-CdSe seeds and CdSe/CdS nanorods. (a) w-CdSe seeds, (b) CdSe/CdS nanorods with length 12 nm and diameter 4.7 nm; (c) CdSe/CdS nanorods with length 46 nm and diameter 4.2 nm. **(right)** Powder X-ray diffraction spectra of zb-CdSe seeds and CdSe/CdS nano-tetrapods. (a) zb-CdSe seeds, (b) CdSe/CdS nano-tetrapods with arm length 24 nm and diameter 4.5 nm; (c) CdSe/CdS nano-tetrapods with arm length 38 nm and diameter 4.7 nm. Red and blue stick patterns show bulk reflections of CdSe and CdS, correspondingly.

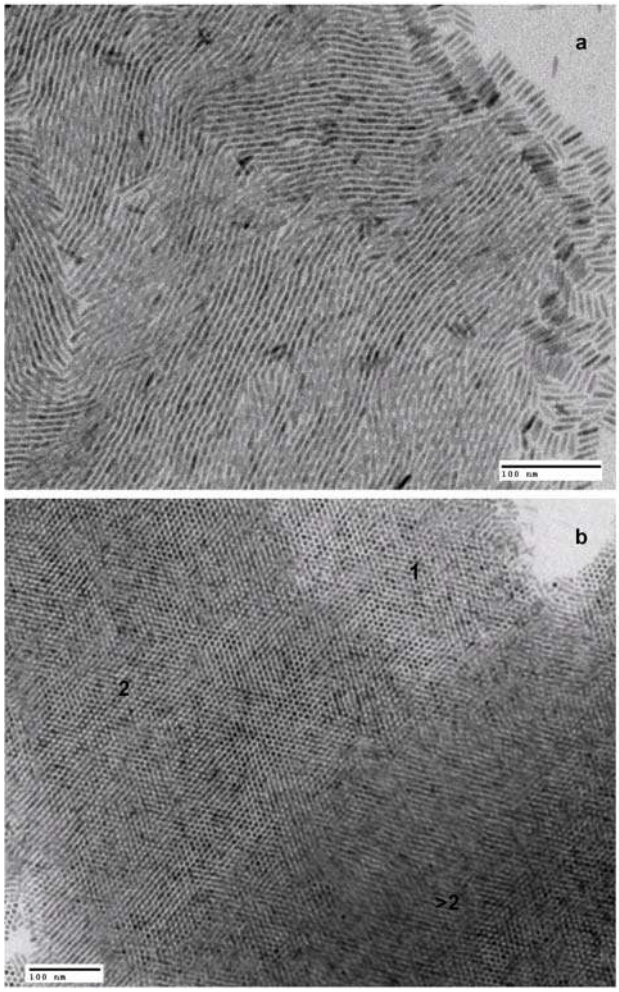

Figure S3. Superstructures of CdSe/CdS nanorods with (a) nematic and (b) long range ordering. Numbers in (b) show the number of layers of vertically aligned nanorods in the superlattice. The image contrast shows the one-on-one stacking of the nanorods in adjacent layers. This structure corresponds to simple hexagonal packing of the nanorods.

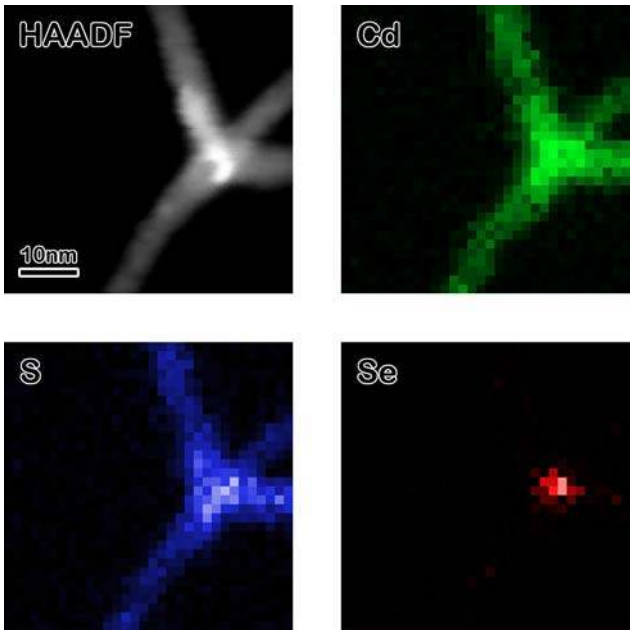

Figure S4. The elemental map showing distribution of Cd, S and Se in the nano-tetrapod. The elemental map was obtained by recording 2-D map of EDS signal intensities. High resolution TEM and high angle annular dark field scanning transmission microscopy (HAADF STEM) studies and mapping of the elements were performed using JEOL 2100-F 200 kV Field-Emission Analytical Transmission Electron Microscope equipped with an Oxford energy dispersive x-ray spectrometer (EDS) and Gatan imaging filter for energy loss spectroscopy (EELS).

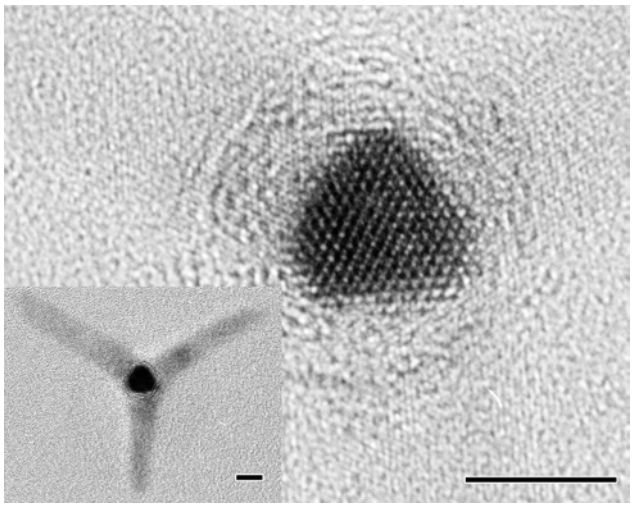

Figure S5. HRTEM image of a central part of CdSe/CdS nano-tetrapod showing arm faceting. Scale bars, 5 nm

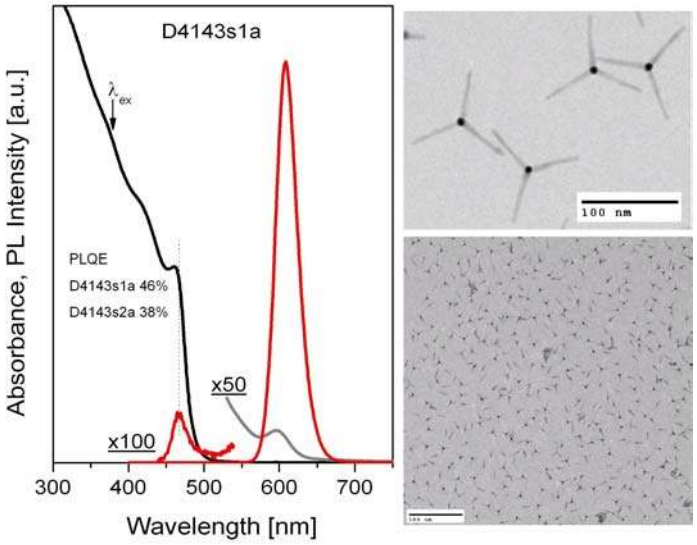

Figure S6. Absorption (black) and PL (red) spectra of toluene solutions of CdSe/CdS nano-tetrapods with 50 nm long arms grown from 3.6 nm zb-CdSe seeds. Gray line shows magnified absorption spectrum to emphasize structure of the absorption onset. Roght panel shows corresponding TEM images.